

Density Profiles of Collisionless Equilibria. II. Anisotropic Spherical Systems

Eric I. Barnes

Department of Physics, University of Wisconsin—La Crosse, La Crosse, WI 54601

barnes.eric@uwlax.edu

Liliya L. R. Williams

Department of Astronomy, University of Minnesota, Minneapolis, MN 55455

llrw@astro.umn.edu

Arif Babul¹

Department of Physics & Astronomy, University of Victoria, BC, Canada

babul@uvic.ca

Julianne J. Dalcanton²

Department of Astronomy, University of Washington, Box 351580, Seattle, WA 98195

jd@astro.washington.edu

ABSTRACT

It has long been realized that dark matter halos formed in cosmological N-body simulations are characterized by density profiles $\rho(r)$ that, when suitably scaled, have similar shapes. Additionally, combining the density and velocity dispersion profiles $\sigma(r)$, each of which have decidedly nonpower-law shapes, leads to quantity ρ/σ^3 that is a power-law in radius over 3 orders of magnitude in radius. Halos' velocity anisotropy profiles $\beta(r)$ vary from isotropic near the centers of halos to quite radially anisotropic near the virial radius. Finally, there appears to be a nearly linear correlation between β and the logarithmic density slope γ for a wide variety of halos. This work is part of a continuing investigation of the above interrelationships and their origins using analytical and semi-analytical techniques. Our findings suggest that the nearly linear β - γ relationship is not just another expression of scale-free ρ/σ^3 behavior. We also note that simultaneously reproducing density and anisotropy profiles like those found in simulations requires $\beta(r)$ and $\gamma(r)$ to have similar shapes, leading to nearly linear

¹Leverhulme Visiting Professor, Universities of Oxford and Durham

²Alfred P. Sloan Foundation Fellow

β – γ correlations. This work suggests that the β – γ and power-law ρ/σ^3 relations have distinct physical origins.

Subject headings: dark matter — galaxies:structure — galaxies:kinematics and dynamics

1. Introduction

Cosmological N-body simulations are important tools that allow us to reconstruct how gravitationally bound objects like galaxies and clusters form and evolve in the universe. The base-level simulations involve Newtonian gravitational interactions between particles that represent masses of dark matter exclusively. These types of simulations suppress the short-range interactions between masses, making the dynamics collisionless, *i.e.*, particles move under the influence of a global potential. The consensus view of the results of such simulations is that all bound structures have common density structures determined by a few parameters. The most often discussed density distribution in the literature is the empirical Navarro-Frenk-White (Navarro, Frenk, & White 1996, 1997, NFW) function. However, many different functions have been invoked to describe the density profiles of dark matter structures resulting from individual simulations (*e.g.*, Sérsic 1968; Moore *et al.* 1998; Navarro *et al.* 2004). While there is a considerable amount of literature attempting to explain the universality of N-body density profiles (Syer & White 1998; Lokas 2000; Nusser 2001; Barnes *et al.* 2005; Lu *et al.* 2006), no widely accepted explanation exists.

We are looking to gain a fundamental understanding of the physics driving the universality of dark matter halos in collisionless simulations. Such insight may eventually provide a way of reconciling the differences between simulated halos and the inferred properties of halos of observed galaxies, such as the cusp–core controversy (*e.g.*, de Blok, McGaugh, & Rubin 2001; Spekkens, Giovanelli, & Haynes 2005). However, the results of the present paper cannot be directly applied to observed galaxies and clusters because the latter are affected by dissipational baryonic processes, which we ignore in the present work; we concentrate exclusively on the effects of gravity in collisionless systems.

In the past few years, two interesting relationships have been uncovered that link various dynamical properties of halos formed in simulations like those discussed above. Taylor & Navarro (2001) have found that there is a scale-free relationship between a phase-space proxy and radius; $\rho/\sigma^3 \propto r^{-\alpha}$, where ρ is density, σ is velocity dispersion, r is radial distance, and α is a constant for any given halo. Interestingly, this relationship is not unique to N-body results. Austin *et al.* (2005) have shown that halos created semi-analytically also have power-law ρ/σ^3 behavior and speculate that this feature is a result of violent relaxation.

The other relationship relates the density and velocity anisotropy profiles of N-body halos (Hansen & Moore 2004). Specifically, the curve describing the logarithmic radial derivative of the

logarithm of the density has the same basic shape as the radial profile of a halo’s anisotropy. As with the power-law behavior of ρ/σ^3 , there is no obvious basis for this relationship, but together they signal that there are unifying physical processes at work in halo formation.

This paper and its companion (Barnes *et al.* 2006, hereafter Paper I) take steps towards uncovering what these processes are. In that work, we found that the mechanical equilibrium of halos with velocity isotropy is not the cause of power-law ρ/σ^3 profiles, as at least two well-known equilibrium density profiles (Hernquist and King) do not produce ρ/σ^3 power-laws. However, Navarro *et al.* (2004) and Sérsic density distributions in mechanical equilibrium produce nearly scale-free ρ/σ^3 profiles. We have also investigated density profiles that result from solving the isotropic Jeans equation with the constraint that $\rho/\sigma^3 \propto r^{-\alpha}$. In this restricted case, density profiles are similar to those presented in Navarro *et al.* (2004) but are reproduced better by Sérsic models.

We continue and expand this work by again considering the density profiles that result from solving the Jeans equation under the assumption of scale-free ρ/σ^3 (motivated by N-body and semi-analytical results), but now the velocity distributions will not be restricted to be isotropic. The details of solving the “constrained” Jeans equation are given in §2. The anisotropic Jeans equation admits a wide variety of solutions. We use generic, but sensible, forms for our adopted anisotropy profiles. These profiles and the solutions that result are discussed in detail in §3 and 4. Our main conclusion follows from these sections; equilibrium density profiles replicate those seen in simulations if the radial density and anisotropy profiles of any given halo have similar shapes. The degree of connectedness between the ρ/σ^3 and density slope-anisotropy relations is considered in Section 5. We end with a summary of our findings and our conclusions.

2. The Constrained Jeans Equation

The Jeans equation is a moment of the collisionless Boltzmann equation. Where the Boltzmann equation describes the evolution of the full phase-space distribution function, which is not easily obtained from simulations, let alone observations of real galaxies, the Jeans equation relates observationally accessible quantities, like density and velocity dispersion. Mechanical equilibrium for a spherical collisionless system with radially dependent anisotropy is determined through the Jeans equation (Jeans 1919; Binney & Tremaine 1987),

$$\frac{d}{dr} \left[\frac{\rho(r)\sigma^2(r)}{3 - 2\beta(r)} \right] + \frac{2\beta(r)}{3 - 2\beta(r)} \frac{\rho(r)\sigma^2(r)}{r} = -G\rho(r) \frac{M(r)}{r^2}, \quad (1)$$

where $M(r)$ is the mass enclosed at radius r , ρ is the density, σ is the total velocity dispersion, and β is the anisotropy. The $3 - 2\beta(r)$ terms result from our choice to use the total velocity dispersion rather than the r -component. While we do not directly calculate phase-space distribution functions here, the density and velocity dispersion functions that will be discussed are everywhere positive, implying that the corresponding distribution functions are physically plausible.

One can reduce the number of functions in Equation 1 by assuming an “equation of state” that connects the density to the total dispersion. We use the empirically established relation $\rho/\sigma^3 = (\rho_0/v_0^3)(r/r_0)^{-\alpha}$. We note that while this connection is consistent with the available numerical evidence (Taylor & Navarro 2001; Dehnen & McLaughlin 2005), it is not the only choice. One could equally well choose to utilize the radial dispersion, as in Dehnen & McLaughlin (2005). At this point in time, it is not clear which choice is the most physically relevant.

Imposing this scale-free ρ/σ^3 constraint and changing to the dimensionless variables $x \equiv r/r_0$ and $y \equiv \rho/\rho_0$, we rewrite Equation 1 as,

$$-\frac{x^2}{y} \left[\frac{d}{dx} \left(\frac{y^{5/3} x^{2\alpha/3}}{3 - 2\beta(x)} \right) + \frac{2\beta(x)}{3 - 2\beta(x)} y^{5/3} x^{2\alpha/3 - 1} \right] = BM(x), \quad (2)$$

where $B = G/r_0 v_0^2$. Differentiating this equation with respect to x gives us,

$$\frac{d}{dx} \left[-\frac{x^2}{y} \left\{ \frac{d}{dx} \left(\frac{y^{5/3} x^{2\alpha/3}}{3 - 2\beta(x)} \right) + \frac{2\beta(x)}{3 - 2\beta(x)} y^{5/3} x^{2\alpha/3 - 1} \right\} \right] = Cyx^2, \quad (3)$$

where $C = 4\pi\rho_0 r_0^2/v_0^2$. This expression is an extension of equation (8) in Paper I. We eliminate the constant C by solving for y , differentiating with respect to x again, and grouping like terms. The resulting constrained Jeans equation is,

$$\begin{aligned} (2\alpha + \gamma - 6) \left(\frac{2}{3}(\alpha - \gamma) + 1 \right) (2\alpha - 5\gamma) &= 15\gamma'' + 3\gamma'(8\alpha - 5\gamma + 4\beta + 12\beta\delta b_1 - 5) \quad (4) \\ &- 3\delta[b_1(4\alpha^2 + \gamma^2 - 8\alpha\gamma + 8\alpha + 7\gamma - 15)] \\ &- 3\delta^2[6b_1 b_2(\alpha - \gamma + 1)] \\ &- 3\delta^3[b_3(54\beta + 144\beta^2 + 24\beta^3)] \\ &- 3\delta'[6b_1(\alpha - \gamma + 1) + 9b_1 b_2 \delta] - 3\delta''[3b_1] \end{aligned}$$

In this notation, $\gamma = \gamma(x) = -d \ln y / d \ln x$ is the logarithmic density slope, $\delta = \delta(x) = d \ln \beta / d \ln x$, $b_1 = 2\beta/(3 - 2\beta)$, $b_2 = (3 + 2\beta)/(3 - 2\beta)$, $b_3 = (3 - 2\beta)^{-3}$, and the primes indicate derivatives with respect to $\ln x$.

As discussed previously, the parameter α is a constant, and we choose to investigate the following values; $\alpha = 1.875$, $35/18 = 1.94\bar{4}$, 1.975 . These values have been chosen based on the findings of Austin *et al.* (2005). For isotropic systems, $\alpha = 35/18$ represents a critical point for solutions of the constrained Jeans equation. Solutions with $\alpha > 35/18$ have γ values that asymptote to finite values, and $\alpha = 1.975$ is our example of such a case. In terms of density, these solutions approach power-law density profiles at large radius. In the other case, γ values increase indefinitely with radius, implying density profiles that continually steepen farther from the center. Our value of $\alpha = 1.875$ (which is also the value found by Taylor & Navarro (2001)) represents this class of solutions.

While aesthetically unappealing in the extreme, Equation 4 can be straightforwardly solved numerically for γ over a range of $\ln x$ once α and $\beta(x)$ have been specified (different choices of $\beta(x)$

are considered in §§3, 4.1, and 4.2). Our approach to the solution sets $\gamma = 2$ at the scalelength r_0 ($x = 1$). In effect, we define the scalelength of a halo to be the radius where the density slope has the isothermal value. We further define $x_{\text{vir}} = 10$, by analogy with $c = 10$ NFW profiles [note that this does not mean that $\bar{\rho}(x < 10) = 200\rho_{\text{crit}}$]. The remaining initial condition is the value of γ' at r_0 . We leave this as a free parameter to be determined by minimizing the differences between the solution γ -profile and those of the NFW,

$$\begin{aligned}\rho(x)/\rho_0 &= x^{-1}(1+x)^{-2} \\ \gamma(x) &= (1+3x)/(1+x)\end{aligned}\tag{5}$$

and Navarro *et al.* (2004, N04)

$$\begin{aligned}\log[\rho(x)/\rho_0] &= (-2/\mu)(x^\mu - 1) \\ \gamma(x) &= 2x^\mu\end{aligned}\tag{6}$$

density profiles. In particular, for the NFW profile $\gamma'(1) = 0.5$ and for the N04 profile $\gamma'(1) = 2\mu$, where $\mu = 0.17$ (the best-fit value from N04). We have chosen these profiles because of their ability to empirically describe the collisionless halos that form in a wide variety of numerical simulations as well as their relative simplicity, but any other profile could be chosen and analyzed in the same way.

3. Constant Anisotropy Solutions

The simplest type of anisotropy distribution is a constant nonzero value. In this case, equation 4 simplifies considerably as δ and its derivatives disappear. Our work in Paper I deals with the special case of $\beta = 0$. Here, we extend to nonzero, but constant, anisotropies ($-0.2 \leq \beta \leq 1.0$). The relevant constrained Jeans equation is,

$$(2\alpha + \gamma - 6)\left(\frac{2}{3}(\alpha - \gamma) + 1\right)(2\alpha - 5\gamma) = 15\gamma'' + 3\gamma'(8\alpha - 5\gamma + 4\beta - 5).\tag{7}$$

Solutions to this equation extend and agree with our earlier work. In general, solutions to the constant anisotropy constrained Jeans equation do not resemble NFW profiles for any tested combination of constant anisotropy value and α value. On the other hand, the constrained Jeans equation solutions can approximate N04 profiles, at least for isotropic and slightly tangentially anisotropic velocity dispersion distributions. For the solutions that best approximate N04 profiles, the anisotropy value decreases as the α value increases. Figure 2 shows γ profiles for $\alpha = 1.875, \beta = 0.1$ (panel a), $\alpha = 35/18 = 1.94\bar{4}, \beta = -0.1$ (panel b), and $\alpha = 1.975, \beta = -0.2$ (panel c). Even mild radial anisotropy ($\beta \gtrsim 0.3$) drives the solutions to have fairly constant γ profiles, independent of α . Panel d of Figure 2 shows the γ profile for $\alpha = 1.875, \beta = 0.5$. We note that the special value $\alpha = 35/18$ is obtained analytically only for $\beta = 0$ (Austin *et al.* 2005). For nonzero constant β , the special value of α can be found by setting the γ' term in Equation 7 equal to zero and utilizing the

relationship for power-law density profiles, $\gamma_{\text{pl}} = 6 - 2\alpha$. The result is that $\alpha_{\text{special}} = 35/18 - 2\beta/9$ (see also Dehnen & McLaughlin 2005).

4. Solutions for Anisotropy Distributions

On relaxing the constant anisotropy requirement, we are immediately faced with a decision. What form should the anisotropy distribution $\beta(x)$ take? We have chosen two flexible functions to investigate; one is a simple power-law while the other is based on the hyperbolic tangent function. For both functions, we choose boundary anisotropy values and we have parameters that affect the rates of change between these boundary values. The functions are similar in that they both monotonically increase with $\ln x$, following the stability argument given in Merritt & Aguilar (1985). As the next two subsections will show, the important difference between the two functions is that the power-law has a positive second derivative everywhere while the hyperbolic tangent has an inflection point.

Specifically, the power-law function is given by,

$$\beta(x) = \beta_{\text{lo}} + (\beta_{\text{hi}} - \beta_{\text{lo}}) \left[\frac{\ln x + \ln x_{\text{bound}}}{\ln x_{\text{vir}} + \ln x_{\text{bound}}} \right]^\eta, \quad (8)$$

where β_{lo} is the anisotropy value as $\ln x \rightarrow -\ln x_{\text{bound}}$, β_{hi} is the anisotropy value at the scaled virial radius x_{vir} , $\eta > 0$ controls the shape of the distribution, and the range of integration is determined by $\ln x_{\text{bound}} = 25$. We fix the scaled virial radius at the value for an NFW halo with a concentration index of 10, $x_{\text{vir}} = 10$. While our solutions cover large ranges of x , we will be interested primarily in the several orders of magnitude surrounding the scalelength.

The other distribution that we study will be referred to as the tanh anisotropy profile. The expression for this distribution is,

$$\beta(x) = \frac{1}{2}(\beta_{\text{hi}} - \beta_{\text{lo}})[1 + \tanh(s \ln x)] + \beta_{\text{lo}}, \quad (9)$$

where again β_{lo} is the anisotropy as $\ln x \rightarrow -\ln x_{\text{bound}}$, β_{hi} is now the anisotropy as $\ln x \rightarrow \ln x_{\text{bound}}$, and s determines the rate of change between these boundary values. Now, $\tanh z = (e^z - e^{-z})/(e^z + e^{-z})$ and $1 + \tanh z = 2e^z/(e^z + e^{-z})$. If $z = s \ln x = \ln x^s$, then $1 + \tanh z = 2x^s/(x^s + x^{-s}) = 2x^{2s}/(x^{2s} + 1)$. The tanh form is thus a generalization of commonly discussed anisotropy functions; $\beta \propto r^2/(r^2 + r_a^2)$ (Osipkov-Merritt) for $s = 1$, and $\beta \propto r/(r + a)$ (*e.g.*, Mamon & Lokas 2005) for $s = 1/2$. The tanh form we adopt allows for more flexibility in the anisotropy profile.

Our approach to solving Equation 4 with these anisotropy distributions is as follows. First, choose a profile type to fit to; either the NFW or N04 γ distribution. Next, choose pairs of $(\beta_{\text{lo}}, \beta_{\text{hi}})$ values. With the boundary anisotropy values fixed, we are left with one free parameter in each β profile. For each set of $(\beta_{\text{lo}}, \beta_{\text{hi}})$, we find the η or s that minimizes the average least-squares difference between the γ profile that results from solving Equation 4 and the chosen γ distribution

over the range $10^{-3}x_{\text{vir}}$ and x_{vir} , a range over which N-body simulations produce meaningful results. This procedure provides us with the best approximation to either the NFW or N04 profiles given a set of boundary anisotropy values. Note that we do not use the least-squares values for hypothesis testing or for making statistical comparisons between the various anisotropy forms, but rather to find the form of the anisotropy profile that best reproduces NFW/N04 density profiles, while solving the Jeans equation.

4.1. Power-law Anisotropy Solutions

For the power-law anisotropy solutions, we have investigated a parameter space with $0.0 \leq \beta_{\text{lo}} \leq 0.9$ and $0.1 \leq \beta_{\text{hi}} \leq 1.0$. Points where $\beta_{\text{lo}} = \beta_{\text{hi}}$ have not been included as they are identical to the constant anisotropy models (§3). Points with $\beta_{\text{lo}}, \beta_{\text{hi}} < 0$ have been excluded due to an instability in the fitting routine for these models. We have also investigated the regions of parameter space where $\beta_{\text{lo}} > \beta_{\text{hi}}$, but those fits are uniformly uninteresting as the solutions do not resemble any sort of physically relevant density profile. The solutions which best match NFW and N04 profiles all have $\beta_{\text{lo}} = 0$. Solutions that are matched to NFW profiles tend to have smaller best-fit β_{hi} values than those matched to N04 profiles. The best-fit solutions are discussed in detail below.

The best-fit γ distributions with power-law anisotropy profiles are shown in Figure 3, where the solutions (solid lines) are matched to the NFW profile (dashed lines). Dash-dotted lines illustrate N04 γ profiles. Dotted lines show the anisotropy profile from Mamon & Lokas (2005). Panels a and b show the γ and β profiles calculated with $\alpha = 1.875$ that best match the appropriate profile, panels (c, d) and (e, f) illustrate the same distributions, but for $\alpha = 35/18$ and $\alpha = 1.975$, respectively. Note that the solutions for the power-law anisotropy profile never resemble the NFW profile; *i.e.*, the best-fits are not good fits.

Figure 4 illustrates the same relations, but the solutions are matched to the N04 profile. The line styles are the same as in Figure 3. The N04 profile is reproduced with much greater accuracy than the NFW profile, but the match becomes substantially worse as α increases. Note that for the solutions that match the N04 profiles, the best-fit anisotropy profile has an isotropic distribution near the center and a highly radial anisotropic character ($0.8 \lesssim \beta \lesssim 1.0$) near the virial radius. This character of anisotropy profiles has been noted previously in N-body simulations (*e.g.*, van Albada 1982; Cole & Lacey 1996). It has also been suggested that such behavior is evidence that an orbital stability process is at work in determining the density structure of equilibrium halos (Barnes *et al.* 2005).

In numerous N-body simulations, a nearly linear relationship has been found between the anisotropy and density-slope profiles (Hansen & Moore 2004, 2006). It is important to note that no one simulation displays an exactly linear β - γ profile. Over the range of γ values our solutions cover ($1 \lesssim \gamma \lesssim 3$), individual simulation β - γ curves are nearly linear indicating that the anisotropy

and density slope distributions have similar shapes. The variations present in Figure 2 of Hansen & Moore (2006) appear to originate from differing slopes and intercepts for different simulations.

In Figures 5 and 6, we present the β vs. γ profiles (solid lines) obtained from the solutions shown in Figures 3 and 4 and compare them to the relations found in N-body simulations. The dashed lines represent the mean trend of the simulation results and the dash-dotted lines show the extent of variations in those results. Of the six curves in Figures 5 and 6, the best qualitative match to the near-linear relationship found in Figure 2 of Hansen & Moore (2006) is given by the N04-like profile with $\alpha = 1.875$, but other values $1.8 \lesssim \alpha \lesssim 1.9$ would also give similar results (Figure 6a). One difference is that our relation is “steeper”; we reach total radial anisotropy at $\gamma = 3$, while the mean simulation results reach $\beta \approx 0.5$ at $\gamma = 3$. Solving the constrained Jeans equation for N04-like profiles with $\alpha \gtrsim 1.9$ or for NFW-like profiles does not produce near-linear β – γ relations, but the solutions are at least consistent with the mean trend within the variations seen in simulations.

4.2. Tanh Anisotropy Solutions

We now turn to the hyperbolic tangent (tanh) anisotropy distribution solutions. The parameter space for the tanh profile is slightly different than for the power-law anisotropy distribution; $-0.2 \leq \beta_{\text{lo}} \leq 0.9$ and $0.3 \leq \beta_{\text{hi}} \leq 1.0$. Other combinations of β_{lo} and β_{hi} yield unrealistic density profiles. As in the power-law case, the β_{lo} values for the solutions that best match both NFW and N04 profiles are small, $\beta_{\text{lo}} \leq 0.1$. The β_{hi} values for the NFW matched solutions are larger than those for the N04 matched solutions. The specifics of the best-fit solutions are given below.

The solutions that best approximate the NFW profile have anisotropy profiles that vary from isotropic near the center to mildly radially anisotropic ($\beta \gtrsim 0.5$) at the virial radius. The best-fit solutions’ γ and β profiles are shown in Figure 7. Again, the line styles are the same as in Figure 3. Unlike in the power-law β case, it is easy to see that these solutions approximate the asymptotic NFW behavior quite well.

Another difference from the power-law case is the behavior of the solutions that resemble N04 profiles. These solutions tend to have fairly constant anisotropy distributions that are nearly isotropic ($\beta \lesssim 0.3$). This is most evident when we look at the best-fit solution γ and β profiles in Figure 8. The N04 γ profile is well-fit by the solution, but only when the anisotropy profile is nearly constant near zero. This agrees with the work presented in Paper I where a $\beta = 0$ profile produces solutions that are good approximations to N04 profiles.

Figures 9 and 10 show the β vs. γ curves for the NFW-like and N04-like solutions, respectively. The curve for the NFW-like solution with $\alpha = 1.875$ (Figure 9a) is remarkably linear, again indicating the similarity of the β and γ distributions. In fact, each of the curves in Figure 9 have substantial regions of linearity. This behavior makes them all qualitatively similar to the results of Hansen & Moore (2006) (marked by the dashed and dash-dotted lines as before). However, the

most linear relation (panel a with $\alpha = 1.875$) is also the one that disagrees most strongly with the simulation results. The remaining profiles ($\alpha = 1.94\bar{4}$ and $\alpha = 1.975$) actually show a decent quantitative match to the mean simulation trend. Figure 10 shows that the N04-like density profile that is most linear (again $\alpha = 1.875$) is a poor quantitative match to simulation results. Overall, the N04-like density profiles produce nearly horizontal β – γ profiles, qualitatively dissimilar to the profiles from simulations. However, we note that profiles created with larger ($\gtrsim 1.94\bar{4}$) α values are quantitatively consistent with simulations.

5. Relating Scale-free ρ/σ^3 and β vs. γ

As these results have been found by assuming the power-law nature of ρ/σ^3 , one could ask whether or not the β vs. γ behavior is independent of scale-free ρ/σ^3 . Since there is no known theoretical motivation for either of these relationships, we attack this question with different tactics.

The extended secondary infall model (ESIM) (Williams, Babul, & Dalcanton 2004; Austin *et al.* 2005) is a semi-analytical halo formation scenario based on the work of Ryden & Gunn (1987). In ESIM, spherical halos form by accreting shells of material that have decoupled from Hubble expansion. These halos exist at overdense locations and their formation includes effects from secondary perturbations that can be completely specified and controlled. As shells collapse, the shells’ energies change in response to the continually changing potential. In fact, the ESIM halo collapse process is best described as violent relaxation because direct two-body effects do not take place (there are no shell-shell interactions), while the shells are allowed to exchange energy by interaction with the global potential. In general, ESIM halos have power-law density distributions over the radial ranges in which N-body simulations show decidedly non-power law behavior, *e.g.*, where NFW profiles change from $\rho \propto r^{-1}$ to $\rho \propto r^{-3}$.

Standard ESIM halos have scale-free ρ/σ^3 (Austin *et al.* 2005; Barnes *et al.* 2005), but what do their β vs. γ curves look like? Panel a of Figure 11 represents the β and γ values taken from a standard ESIM halo, and the locus bears no resemblance to the linear relation found in N-body simulations. This implies that the β – γ relationship is not just a manifestation of a scale-free ρ/σ^3 . It is certainly possible that the process responsible for creating scale-free ρ/σ^3 is not fully expressed in standard ESIM simulations, leading to a different β – γ relationship. However, we suggest that the near-linear relation between β and γ supports an earlier argument that one generic outcome of mostly-radial collapses is an instability that produces velocity distributions with nearly isotropic cores and more radially anisotropic envelopes (Barnes *et al.* 2005). Due to the semi-analytical nature of the ESIM formalism, this instability cannot develop in ESIM halos. However, by manipulating the secondary perturbations present in ESIM halo formation, one can induce this type of anisotropy profile in ESIM halos. Doing so radically changes the associated density profile from the single power-law of the standard halo to an NFW-like form (Barnes *et al.* 2005). These changes strongly affect the overall shape of the β vs. γ plot. Panel b of Figure 11 illustrates the β vs. γ relationship for an NFW-like ESIM halo. While the points certainly do not

fall on a line, they more closely approximate the N-body simulation results. The implication is that the physics driving the density profile shape is also important to establishing the linear β - γ relationship.

6. Summary & Conclusions

It is well-established empirically that ρ/σ^3 is a power-law in radius for virialized, collisionless halos (Taylor & Navarro 2001; Austin *et al.* 2005; Dehnen & McLaughlin 2005). We exploit this relationship and transform the usual Jeans equation into the constrained Jeans equation, solely in terms of the logarithmic density slope γ and the anisotropy β . Doing this allows us to solve directly for γ once an anisotropy distribution has been chosen.

In an earlier paper, Barnes *et al.* (2006), we discussed the solutions of this constrained Jeans equation when the anisotropy is assumed to be zero everywhere. Here, we have extended our earlier work to include constant, but nonzero, anisotropies as well as anisotropy distributions. In particular, we have looked at two flexible, but distinct, types of anisotropy distributions; a power-law and a hyperbolic tangent. We find that, in general, the solutions of the constrained Jeans equation that most resemble the empirical NFW and N04 density profiles have $\beta_{\text{lo}} \approx 0$ and $\beta_{\text{hi}} \gtrsim 0.5$. Anisotropy must be an increasing function of radius in halos like the ones produced in N-body simulations.

A central conclusion of our present work is that there is a distinct similarity between the shapes of radial density and anisotropy profiles. Density profiles that best match the NFW form are found when the anisotropy profile is of the tanh form (right panels of Figure 7), which contains the Osipkov-Merritt and Mamon-Lokas forms as special cases. N04-like solutions are found with either profile (right panels of Figures 4 and 8), but with the tanh β profile, the anisotropy must be roughly constant over the range $10^{-3}r_{\text{vir}} < r < r_{\text{vir}}$ (Figure 8).

Another aspect of this profile similarity is given by the β vs. γ plots (Figures 5, 6, 9, and 10). The combination of β and γ profiles that produce the most linear curves (as suggested by the results of N-body simulations; Hansen & Moore 2004, 2006), are, of course, those profiles that resemble each other most closely. The inflection point in the tanh anisotropy distribution also appears in the NFW density slope distribution (right panels of Figure 7 and Figure 9). In other words, when this second-derivative symmetry is lost, as with NFW-like density and power-law anisotropy profiles (right panels of Figure 3), so is the near-linear correlation between β and γ . However, we note that the most linear β - γ relations found here are also those that are the most quantitatively different from the results of simulations, in that the solid red lines in Figures 6a and 9a extend outside the simulation uncertainty range. This suggests that the relationship between β and γ for any single halo is not strictly linear.

Utilizing the results of semi-analytic models of halo formation, we argue that the β - γ relationship is not just a manifestation of a scale-free ρ/σ^3 . Rather, a near-linear relation between β and γ supports an earlier argument regarding the nature of halo density profiles (Barnes *et al.* 2005).

Velocity distributions with nearly isotropic cores and more radially anisotropic envelopes result from radial collapses. This form of anisotropy distribution necessarily creates a density profile that is less steeply rising in the central regions, since there are fewer radial orbits that plunge close to the center and can support a strong cusp. Likewise, more tangential orbits in the outer regions would increase the density since the average time an orbit spends far from the center would increase. At least in a qualitative sense, this picture supports the observed similarities between profile shapes; more isotropy (smaller β) implies less steeply varying density (smaller γ) and vice versa.

The outcome of this work is that there appear to be at least two physical processes at work in the formation of collisionless dark matter halos in N-body simulations. The evidence presented suggests that one process creates the scale-free ρ/σ^3 distribution and must be a fairly generic collapse process as the ρ/σ^3 behavior is seen in the more restrictive ESIM halos. As a consequence, another process links the anisotropy and density profiles in a unique, nearly linear way.

We thank an anonymous referee for several helpful suggestions. This work has been supported by NSF grant AST-0307604. Research support for AB comes from the Natural Sciences and Engineering Research Council (Canada) through the Discovery grant program. AB would also like to acknowledge support from the Leverhulme Trust (UK) in the form of the Leverhulme Visiting Professorship at the Universities of Oxford and Durham. JJD was partially supported through the Alfred P. Sloan Foundation.

REFERENCES

- Austin, C. G., Williams, L. L. R., Barnes, E. I., Babul, A., Dalcanton, J. J. 2005, ApJ, 634, 756
- Barnes, E. I., Williams, L. L. R., Babul, A., Dalcanton, J. J. 2005, ApJ, 634, 775
- Barnes, E. I., Williams, L. L. R., Babul, A., Dalcanton, J. J. 2006, accepted for publication in ApJ, astro-ph/0510332
- Binney, J., Tremaine, S. 1987, Galactic Dynamics, (Princeton:Princeton Univ. Press)
- Cole, S., Lacey, C. 1996, MNRAS, 281, 716
- de Blok, W. J. G., McGaugh, S. S., Rubin, V. C. 2001, AJ, 122, 2396
- Dehnen, W., McLaughlin, D. E. 2005, MNRAS, 363, 1057
- Hansen, S. H., Moore, B. 2004, astro-ph/0411473
- Hansen, S. H., Moore, B. 2006, NewA, 11, 333
- Jeans, J. H. 1919, Phil. Trans. Roy. Soc. London A, 218, 157

- Lokas, E. L., 2000, MNRAS, 311, 423
- Lu, Y., Mo, H. J., Katz, N., Weinberg, M. D. 2006, MNRAS, 401
- Mamon, G. A., Lokas, E. L. 2005, MNRAS, 363, 705
- Merritt, D., Aguilar, L. 1985, MNRAS, 217, 787
- Moore, B., Governato, F., Quinn, T., Stadel, J., Lake, G. 1998, ApJ, 499, L5
- Navarro, J. F., Frenk, C. S., White, S. D. M. 1996, ApJ, 462, 563
- Navarro, J. F., Frenk, C. S., White, S. D. M. 1997, ApJ, 490, 493
- Navarro, J. F., Hayashi, E., Power, C., Jenkins, A. R., Frenk, C. S., White, S. D. M., Springel, V., Stadel, J., Quinn, T. R. 2004, MNRAS, 349, 1039
- Nusser, A., 2001, MNRAS, 325, 1397
- Ryden, B. S., Gunn, J. E. 1987, ApJ, 318, 15
- Sérsic, J. L. 1968, Atlas de Galaxies Australes (Córdoba: Obs. Astron., Univ. Nac. Córdoba)
- Spekkens, K., Giovanelli, R., Haynes, M. P. 2005, AJ, 129, 2119
- Syer, D., White, S. D. M. 1998, MNRAS, 293, 337
- Taylor, J. E., Navarro, J. F. 2001, ApJ, 563, 483
- van Albada, T. S. 1982, MNRAS, 201, 939
- Williams, L. L. R., Babul, A., Dalcanton, J. J. 2004, ApJ, 604, 18

β -type $\beta = 1 - \frac{\sigma_\theta^2}{\sigma_r^2}$	γ - type $\gamma = -\frac{d \ln(\rho/\rho_0)}{d \ln(r/r_0)}$	NFW (Eq. 5)	N04 (Eq. 6)
	constant β S. 3	Fig. 2– γ vs. $\ln x$ quality of fits – poor all α	
power-law β (Eq. 7) S. 4.1	Fig. 3 – γ, β vs. $\ln x$ quality of fits – poor		Fig. 4 – γ, β vs. $\ln x$ quality of fits – excellent
	Fig. 5 – β vs. γ concave shapes marginally consistent with simulations		Fig. 6 – β vs. γ concave shapes marginally consistent with simulations
tanh β (Eq. 8) S. 4.2	Fig. 7 – γ, β vs. $\ln x$ quality of fits – excellent		Fig. 8 – γ, β vs. $\ln x$ quality of fits – good
	Fig. 9 – β vs. γ nearly linear shapes consistent with simulations		Fig. 10 – β vs. γ nearly horizontal shapes marginally consistent with simulations

Fig. 1.— An overview of the models and results presented in this paper. The columns refer to the two types of density profiles discussed here; Navarro-Frenk-White (Navarro, Frenk, & White 1996, 1997, NFW) and Navarro *et al.* (2004, N04). These profiles are described in detail in §2. The rows delineate the three types of anisotropy profiles; constant (§3), power-law (§4.1), and hyperbolic tangent (§4.2). This table is intended to guide the reader through and summarize the various figures and key results.

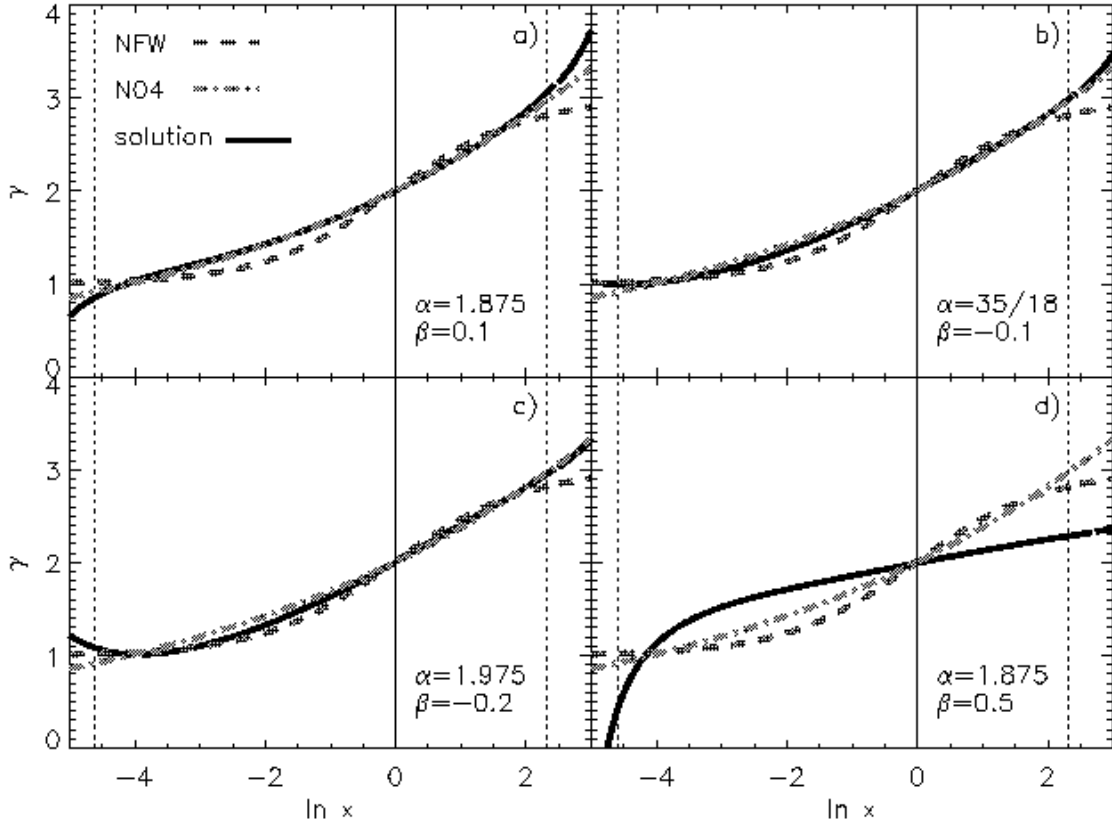


Fig. 2.— The $\gamma = -d\ln(\rho/\rho_0)/d\ln(r/r_0)$ distributions (solid red lines) that result from solving the constrained Jeans equation (Equation 7) with constant anisotropy β values compared with N04 (Equation 6, dash-dotted green lines) and NFW (Equation 5, dashed blue lines) γ profiles. Panels a-c show the solutions that best-fit the N04 profile; no combinations of β and α produced solutions that approximate NFW profiles. Panel a shows the solution with $\alpha = 1.875, \beta = 0.1$. The solution in panel b has $\alpha = 35/18, \beta = -0.1$, and panel c has $\alpha = 1.975, \beta = -0.2$. The solution in panel d has $\alpha = 1.875, \beta = 0.5$. It is included to illustrate the behavior of radially anisotropic systems. All solutions, regardless of α values, with $\beta \gtrsim 0.3$ resemble this solution and provide poor approximations to any empirical γ distribution. See §3 for details.

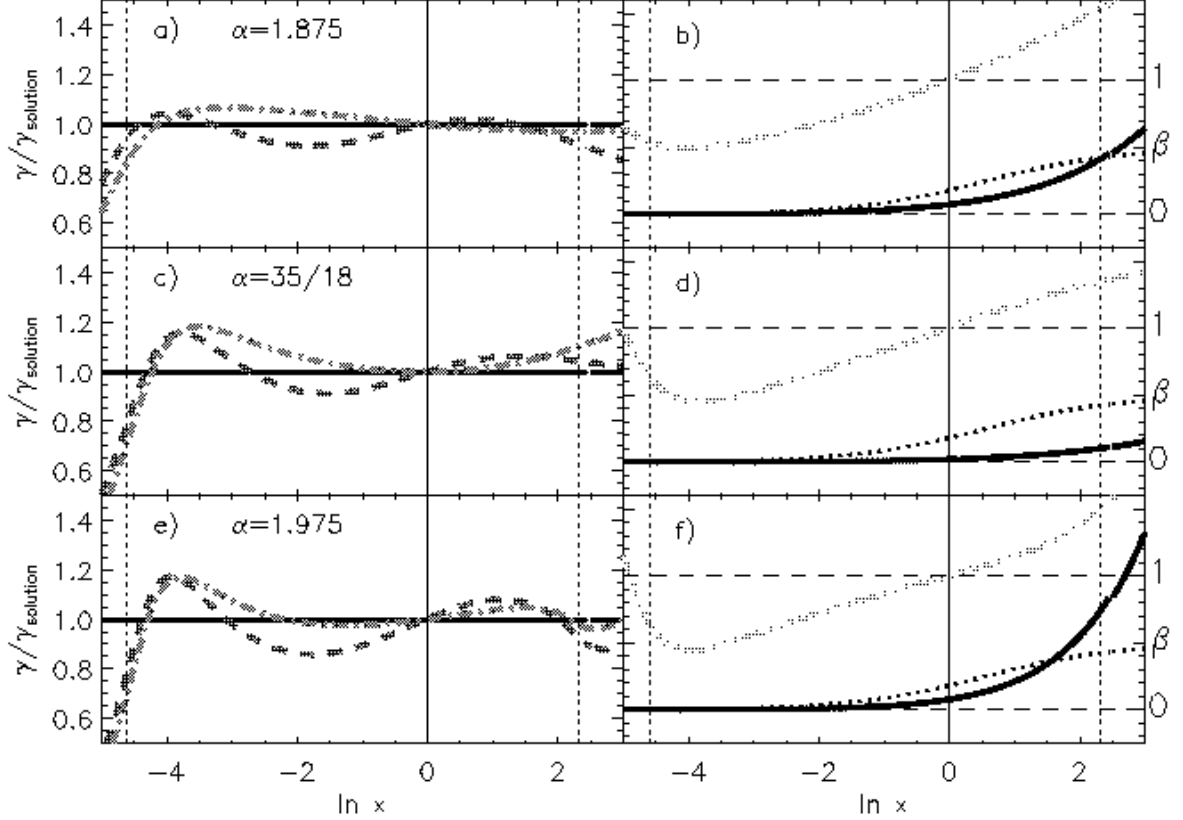


Fig. 3.— With power-law $\beta(x)$, panels a, c, and e show the calculated γ profiles (solid red lines) that best match the NFW γ profile (dashed blue lines) for $\alpha = 1.875$, $35/18$, and 1.975 , respectively. To magnify the variations, each γ profile has been normalized by the solution. The dot-dashed green lines show the N04 γ profile. Panels b, d, and f illustrate the anisotropy distributions used to calculate the solutions (solid red lines). The orange triple-dot-dashed lines are scaled versions of the solution γ profile and are included to compare the shapes of the β and γ profiles. The thick dotted lines represent an anisotropy distribution commonly used to describe the results of N-body simulations (Mamon & Łokas 2005, Equation 60). The vertical dotted lines mark the boundaries of the fitting region, $x = 0.01$ and $x = 10$. The solutions never well-approximate the NFW profile. In fact, for $\alpha = 1.875$, the solution is much more like an N04 profile. Note that an NFW γ profile has an inflection point at $\ln x = 0$, whereas this β profile does not. See §4.1 for details.

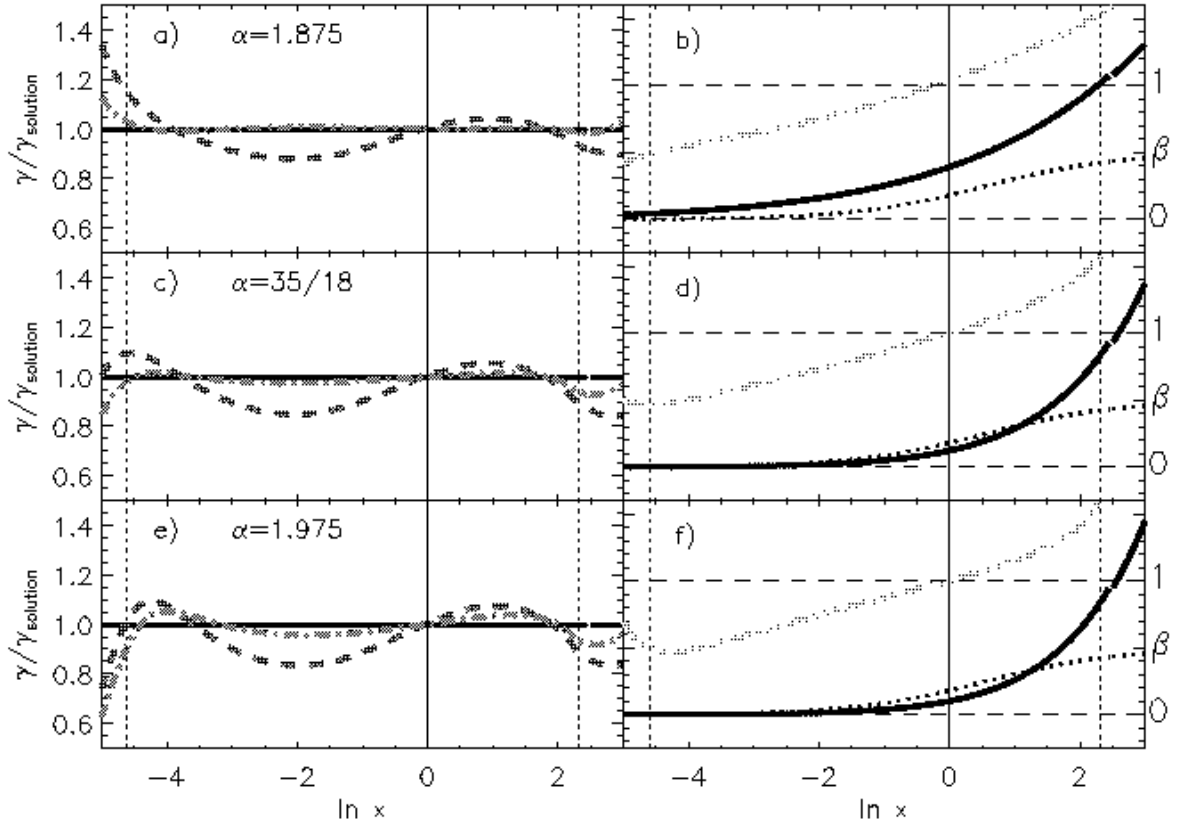


Fig. 4.— With power-law $\beta(x)$, panels a, c, and e show the calculated γ profiles that best match the N04 γ profile for $\alpha = 1.875$, $35/18$, and 1.975 , respectively. Panels b, d, and f illustrate the anisotropy distributions used to calculate the solutions. The line styles are the same as in Figure 3. The solutions match the designated N04 profile reasonably well, in contrast with the results shown in Figure 3.

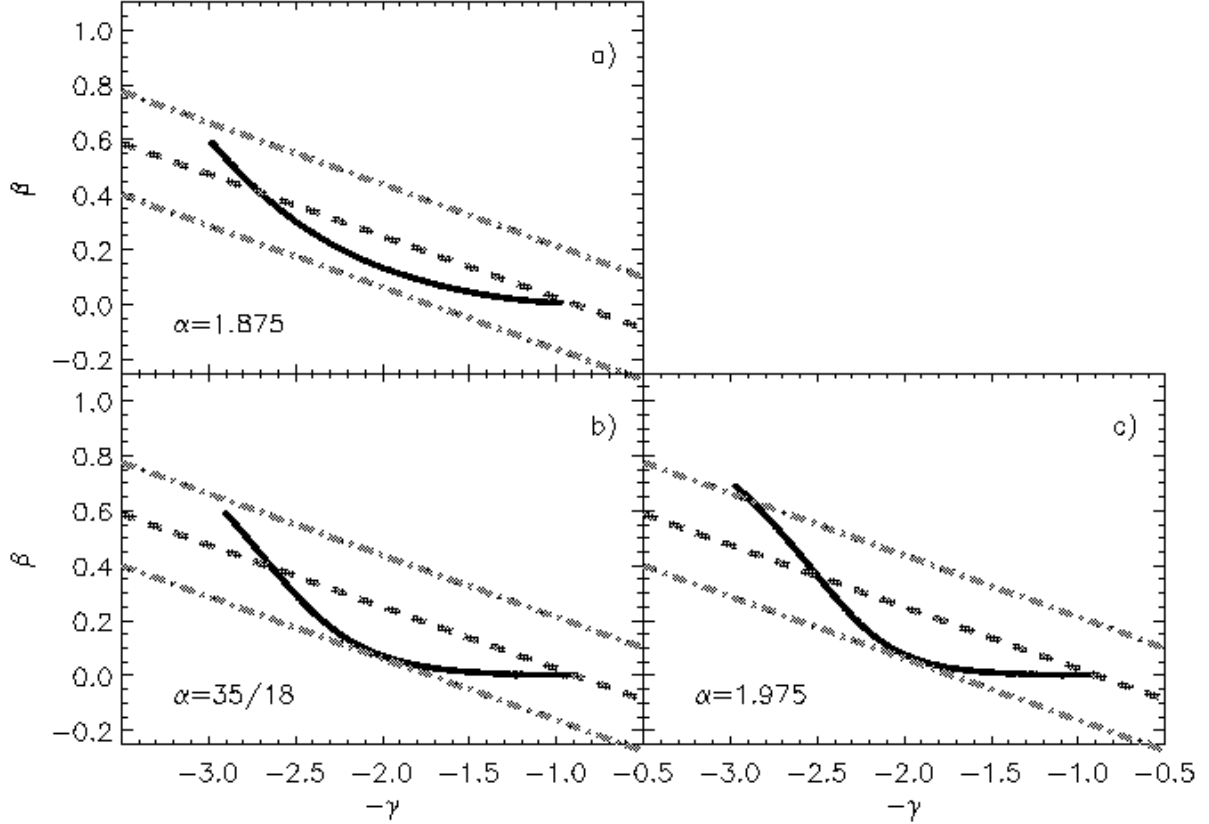


Fig. 5.— Correlations between power-law velocity anisotropy β and logarithmic density slope $-\gamma$ profiles of constrained Jeans equation solutions for $10^{-3}x_{\text{vir}} \leq x \leq x_{\text{vir}}$. Panels a, b, and c represent the best-fit NFW solutions with $\alpha = 1.875$, $35/18$, and 1.975 , respectively. The dashed blue line represents the mean trend found in simulation results (Hansen & Moore 2006) and the dash-dotted green lines mark the extent of variations from those simulations. While the solutions are quantitatively consistent with the simulations, their shapes (particularly the concavity) are unlike the results of simulations over similar ranges of γ values.

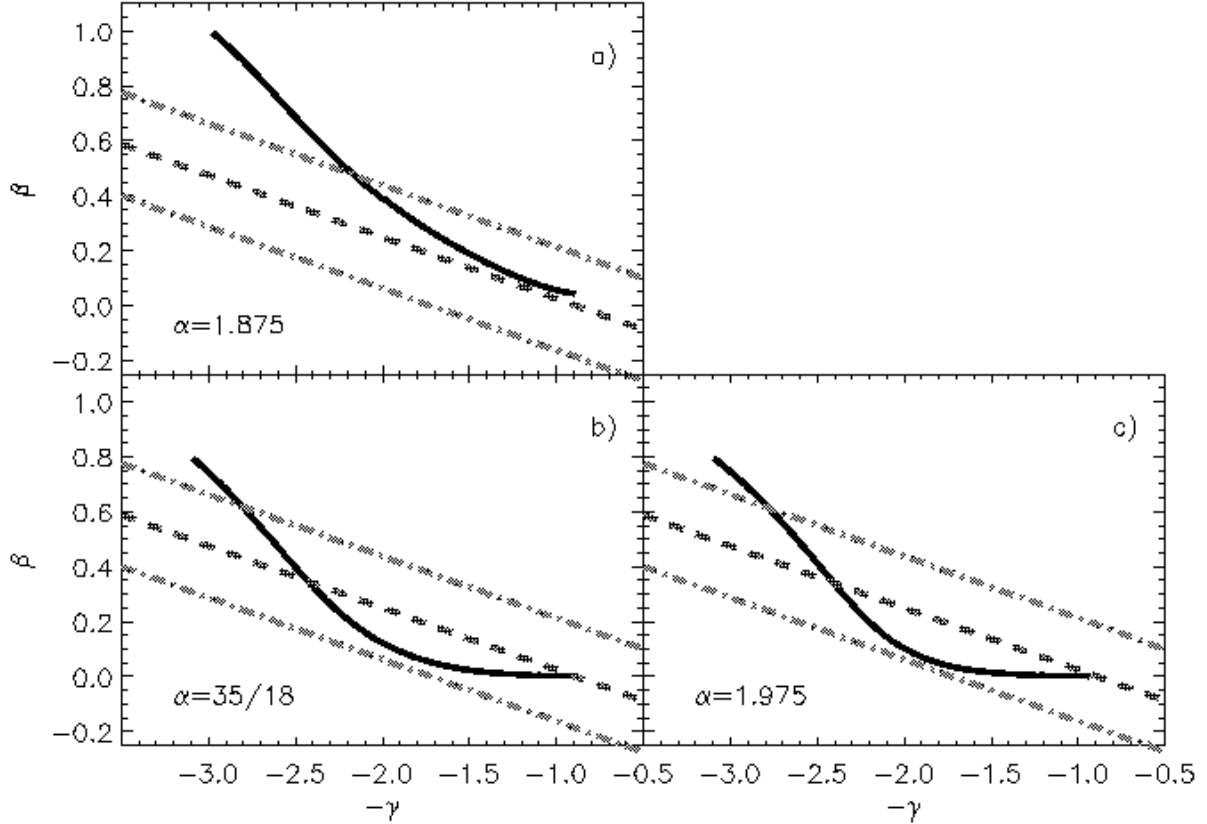


Fig. 6.— Correlations between power-law β and $-\gamma$ solutions for $10^{-3}x_{\text{vir}} \leq x \leq x_{\text{vir}}$. Panels a, b, and c represent the best-fit N04 solutions with $\alpha = 1.875$, $35/18$, and 1.975 , respectively. The dashed blue and dash-dotted green lines are the same as in Figure 5. The most linear (and hence most qualitatively consistent with simulations) relationship in panel a is inconsistent with the quantitative results of simulations. As in Figure 5, the red solution curves that quantitatively agree with simulations have more concavity than the simulations themselves.

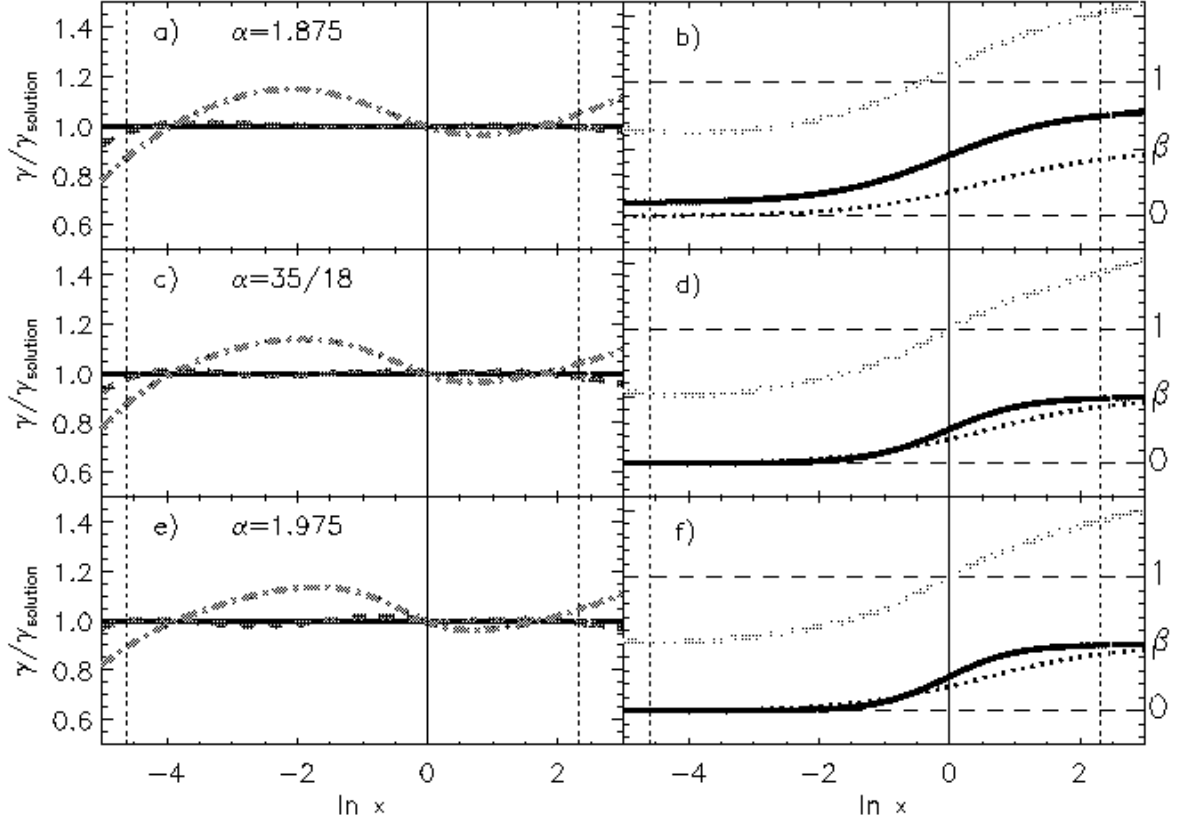


Fig. 7.— With $\tanh \beta(x)$, panels a, c, and e show the constrained Jeans equation solution γ profiles that best match the NFW γ profile for $\alpha = 1.875$, $35/18$, and 1.975 , respectively. Panels b, d, and f illustrate the anisotropy distributions used to calculate the solutions. The line styles are the same as in Figure 3. Unlike the results shown in Figure 3, NFW profiles are reproduced very well by these solutions. Note that now the γ and β profiles share the inflection point behavior at $\ln x = 0$. This similarity of γ and β profile shapes implies a near linear correlation in the β – γ plane (Figure 9). See §4.2 for details.

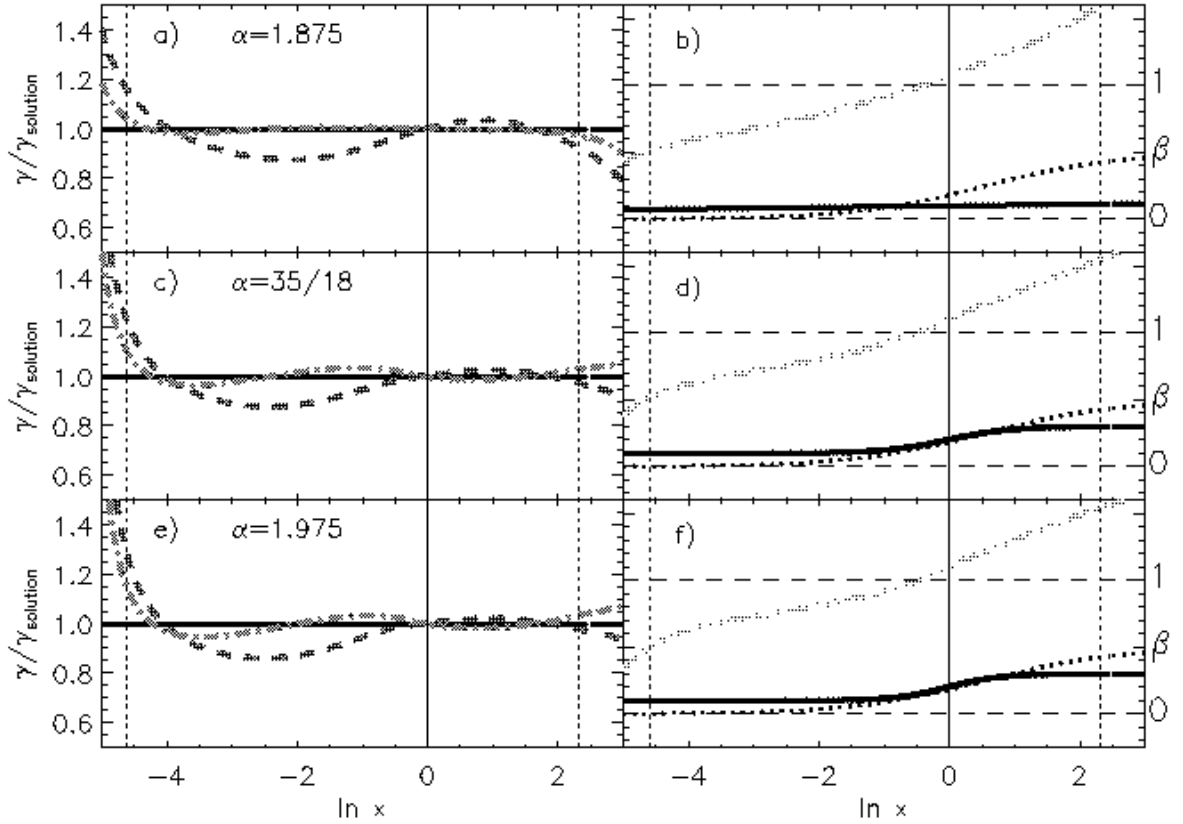


Fig. 8.— With $\tanh \beta(x)$, panels a, c, and e show the calculated γ profiles that best match the N04 γ profile for $\alpha = 1.875$, $35/18$, and 1.975 , respectively. Panels b, d, and f illustrate the anisotropy distributions used to calculate the solutions. The line styles are the same as in Figure 3. These solutions are fair approximations of the designated N04 profile. However, note that the β profiles are nearly horizontal. Higher α values lead to moderate variations in anisotropy, but not as large as those in Figure 7.

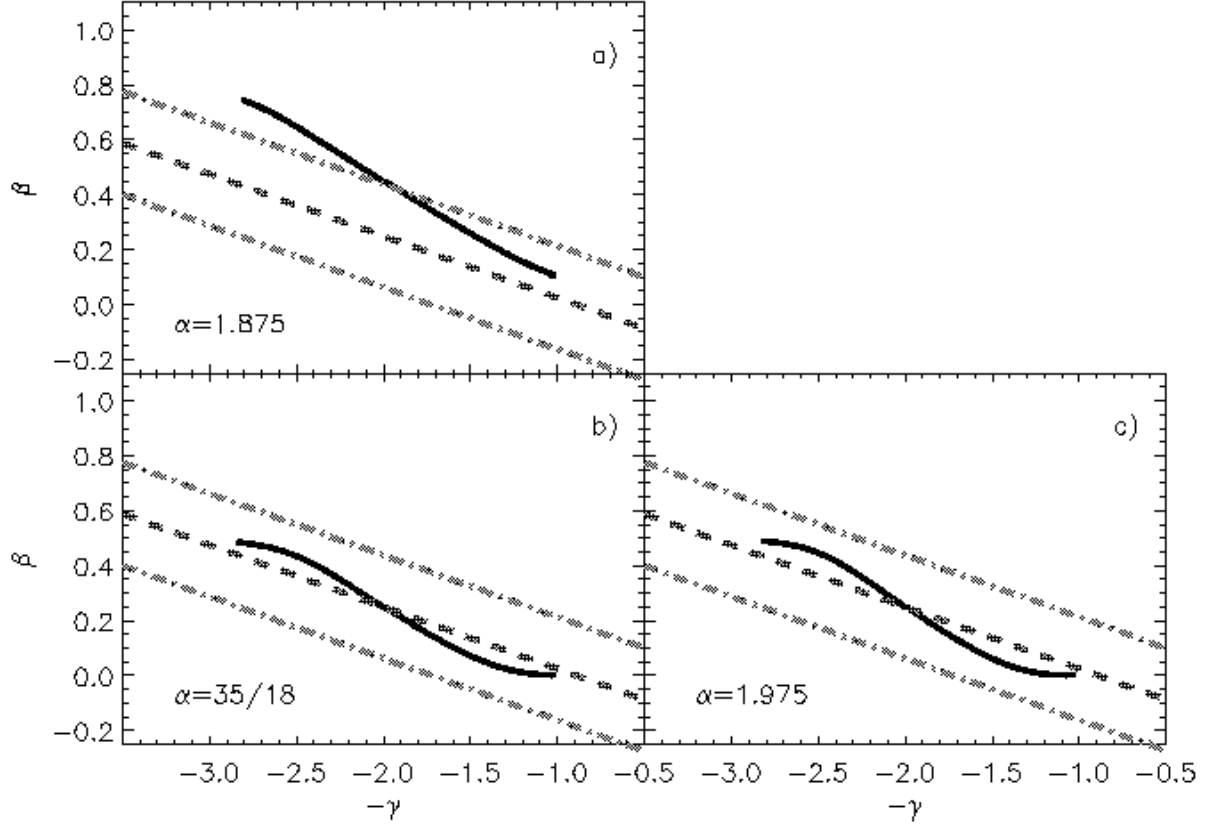


Fig. 9.— Correlations between $\tanh \beta$ and $-\gamma$ for $10^{-3}x_{\text{vir}} \leq x \leq x_{\text{vir}}$. Panels a, b, and c represent the best-fit NFW solutions with $\alpha = 1.875$, $35/18$, and 1.975 , respectively. The dashed blue and dash-dotted green lines are the same as in Figure 5. As in Figure 6, the most linear relation is quantitatively inconsistent with the results of simulations. Higher α values produce red curves that have larger regions of linearity and are consistent with simulations. Recall that in this case the γ and β profiles have similar shapes (particularly the inflection point at $\ln x = 0$).

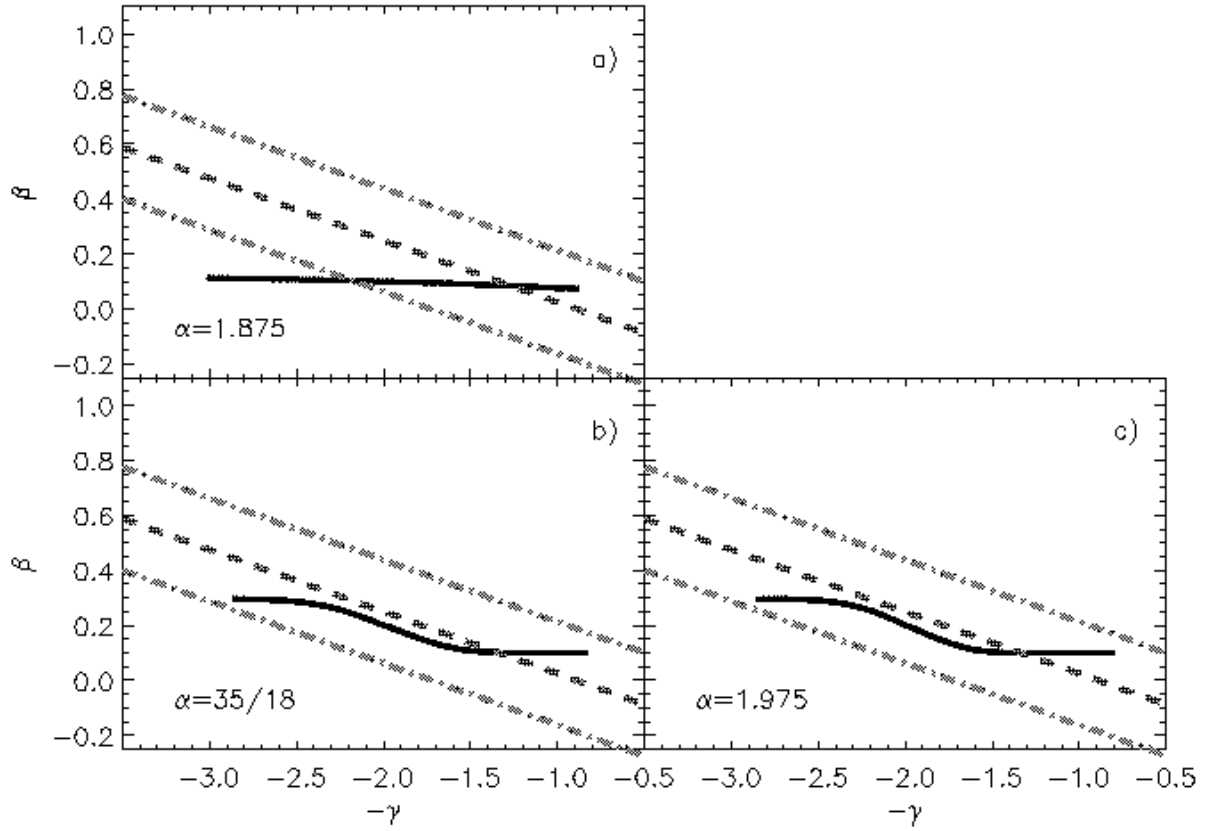


Fig. 10.— Correlations between $\tanh \beta$ and $-\gamma$ for $10^{-3}x_{\text{vir}} \leq x \leq x_{\text{vir}}$. Panels a, b, and c represent the best-fit N04 solutions with $\alpha = 1.875$, $35/18$, and 1.975 , respectively. The dashed blue and dash-dotted green lines are the same as in Figure 5. Overall, the red curves are more horizontal than the simulation results. However, larger α values allow for quantitative agreement between the solution curves and simulations.

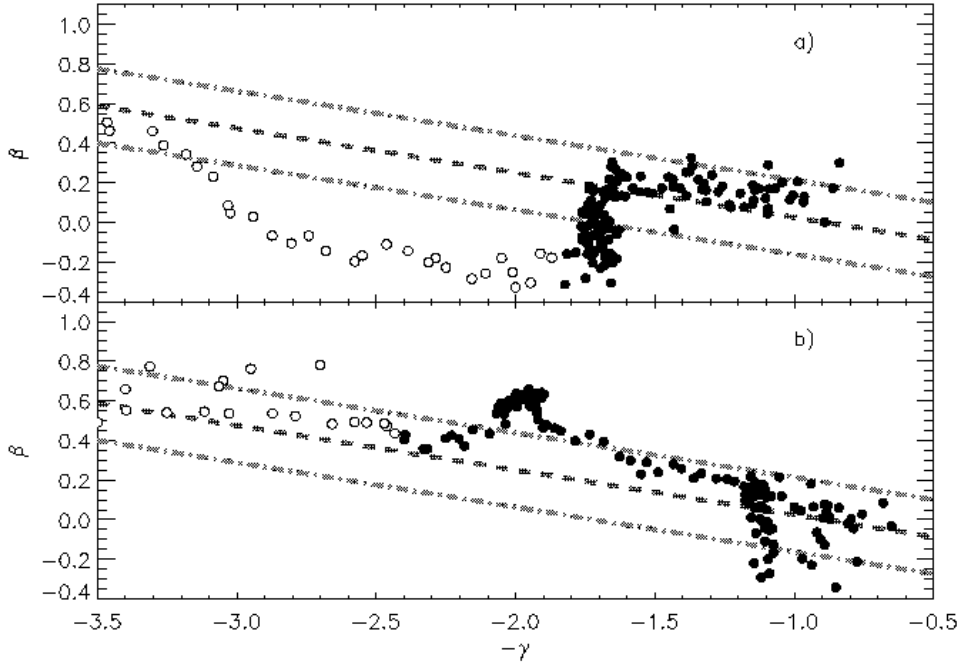


Fig. 11.— The β vs. $-\gamma$ curve for the standard ESIM halo (a). The corresponding curve for the ESIM halo that has been modified so that the density profile resembles that of an NFW model. The points in each panel marked by red solid circles represent parts of the halo that lie in the range $10^{-3} < r/r_{200} < 0$, where r_{200} is the virial radius of those simulations. The open circles lie beyond the virial radius. The dashed blue and dash-dotted green are the same N-body simulation results shown in the previous plots of β vs. γ . Despite the bump at $\gamma = 2$, panel b resembles the results from N-body simulations much more closely than does panel a. Each of these ESIM halos has power-law ρ/σ^3 profiles, but they have radically different γ - β relationships. This suggests that the mechanisms that give rise to each of these relations are independent. The standard halo (panel a) is nearly isotropic out to the virial radius while the NFW-like halo (panel b) has a tanh-like β profile. This prompts us to postulate that the β - γ connection is rooted in the instability that creates isotropic cores and radially anisotropic outer regions, and that the ρ/σ^3 relationship is due to a more general physical process.